

A NOVEL PHANTOM MODEL FOR MOUSE TUMOR DOSE ASSESSMENT UNDER MV BEAMS

Michael S. Gossman,* Indra J. Das,[†] Subhash C. Sharma,[‡] Jeffrey P. Lopez,*
Candace M. Howard,[§] and Pier Claudio[§]

Abstract—In order to determine a mouse's dose accurately and prior to engaging in live mouse radiobiological research, a tissue-equivalent tumor-bearing phantom mouse was constructed and bored to accommodate detectors. Comparisons were made among four different types of radiation detectors, each inserted into the mouse phantom for radiation measurement under a 6 MV linear accelerator beam. Dose detection response from a diode, thermoluminescent dosimeters, and metal-oxide semiconductor field-effect transistors were used and compared to that of a reference pinpoint ionization chamber. A computerized treatment planning system was also directly compared to the chamber. Each detector system demonstrated results similar to the dose computed by the treatment planning system, although some differences were noted. The average disagreement from an accelerator calibrated output dose prescription in the range of 200–400 cGy was $-0.4\% \pm 0.5\sigma$ for the diode, $-2.4\% \pm 2.6\sigma$ for the TLD, $-2.9\% \pm 5.0\sigma$ for the MOSFET, and $+1.3\% \pm 1.4\sigma$ for the treatment planning system. This phantom mouse design is unique, simple, reproducible, and therefore recommended as a standard approach to dosimetry for radiobiological mouse studies by means of any of the detectors used in this study. The authors fully advocate for treatment planning modeling when possible prior to linac-based dose delivery.

Health Phys. 101(6):746–753; 2011

* Tri-State Regional Cancer Center, Radiation Oncology Department, 706 23rd Street, Ashland, KY 41101; [†] Indiana University, School of Medicine, Radiation Oncology Department, 535 Barnhill Drive, RT 041, Indianapolis, IN 46202; [‡] Parkview Comprehensive Cancer Center, Radiation Oncology Department, 11141 Parkview Plaza Drive, Fort Wayne, IN 46845; [§] Marshall University School of Medicine, Department of Biochemistry and Microbiology, Department of Surgery, One John Marshall Drive, BBSC 336-Q, Huntington, WV 25755.

The present studies were supported by National Cancer Institute (NCI) awards CA131395 and CA140024, and in part by *National Institutes of Health* (NIH)-Centers of Biomedical Research Excellence (COBRA) award 5P20RR020180 and West Virginia IDeA Network of Biomedical Research Excellence (WV-INBRE) award 5P20RR016477 (each to PPC). The content is solely the responsibility of the authors and does not necessarily represent the official views of the National Cancer Institute or the National Institute of Health.

For correspondence contact: Michael S. Gossman, Chief Medical Physicist and RSO, Tri-State Regional Cancer Center, Radiation Oncology Department, 706 23rd Street, Ashland, KY 41101, or email at mgossman@tsrcc.com.

(Manuscript accepted 10 March 2011)

0017-9078/11/0

Copyright © 2011 Health Physics Society

DOI: 10.1097/HP.0b013e31821a4838

Key words: accelerators, medical; detector, thermoluminescent; dose assessment; mice

INTRODUCTION

MICE HAVE been used in radiobiological research studies for many years. The original development and use of inbred mice for probing the genetic determinants of resistance and susceptibility to infections and tumors was documented from research by Clara J. Lynch (Morse 1978). During the 1920's, she personally brought a mouse strain into the United States from a laboratory in Lausanne, Switzerland (Lynch 1969). The original population was two males and seven females, which Dr. Lynch kept in a secure shoebox and stored in her stateroom on board the ship.¹ Once at the laboratory of James B. Murphy in the Rockefeller Institute, they were genetically altered in 1937 with a distinctive phenotype (Morse 1978; Leiter 1993; Chia et al. 2005). Now classified *Foxn1^{mm}*, these mice have no body hair (Suzuki et al. 2003). These so-called *nude* mice have a marked ability to engraft many different types of tumor cells from other animals, including humans. Xenografting is a common technique used by radiobiologists to test the characteristics of disease growth, inhibiting drugs, and tumor responses to drugs and radiation by the injection of tumors and drugs into nude mice. An illustration of nude mice subjects is presented in Fig. 1.

Having an immunodeficient research subject is a valuable asset since it removes the single most important degree of freedom: tumor rejection. It is from these studies that novel techniques seen to reduce the size of prostate tumor xenografts have had recent success using drugs injected into mice (Greco et al. 2010). Radiobiologists have valued this animal model for sustained grafted tumor growth, which permits fractionation considerations in therapeutic models, even for radiation therapy (Allam et al. 1995). Almost all radiobiological experiments have been performed with kilovoltage x-ray machines. This is still the primary means of irradiating mouse subjects (Lo



Fig. 1. Foxn1^{nu} (nude) mice with xenografted tumors.

et al. 1993; Gorodetsky et al. 1990). Some research has investigated higher photon energy resulting from ^{137}Cs and ^{60}Co radioactive material irradiators or even radionuclides of ^{90}Y (Lazewatsky et al. 2003; Urano et al. 1998; Agarwal et al. 1975). Linear accelerators have rarely been used in such studies (Kumar et al. 2008; Kuroda et al. 1999; Jaffe et al. 1987). This is due to the fact that radiobiologists have difficulty accessing one, since most medical accelerators approved strictly for human therapy are governed by state level radiation control entities. Still, radiation control branches and inspectors general have provided approval for dual use with immunodepressed nude mice when infectious disease control measures are properly in place. Now that megavoltage modalities are being considered more often, dose rates from x-ray machines and radioactive material at $0.4\text{--}2.5\text{ Gy min}^{-1}$ may now be escalated to pulsed dose rates at $4\text{--}10\text{ Gy min}^{-1}$ from accelerators (Stuben 1994).

In order to determine the dose to a mouse accurately and prior to engaging in live mouse radiobiological research, a tissue-equivalent tumor-bearing mouse phantom was constructed and bored to accommodate detectors. Comparisons were made among four different types of radiation detectors, each inserted into the mouse phantom for radiation measurement (Yorke et al. 2005; Metcalfe et al. 1993; Butson et al. 1996; Quach et al. 2000). The dose levels obtained by each instrument were determined relative to the calibrated x-ray output of a 6 MV accelerator. Detectors were placed individually and consecutively within the mock-up mouse subject and placed in a pie cage duplicating radiobiology research procedures for actual measurement of absorbed dose. An intercomparison of detector-determined dose is presented along with a computerized tomography (CT)-based computerized treatment simulation plan.

MATERIALS AND METHODS

Phantom mouse, pie cage, and detectors

A Braintree Scientific, Inc. (PO Box 361, Braintree, MA 02185) pie cage model MPC with filter model MPC-TP was chosen. As shown in Fig. 2, the acrylic mouse unit is 21.5 cm in diameter and 7.5 cm in height; individual chambers are 5 cm (base) and 9 cm (length). The circular cages secure up to 11 mice in any of 12 wedge-shaped chambers. The notched removable lid can be dialed to any of the ventilated pie-sliced chambers, making it easy to load mice through the single lid opening. This clinical pie cage is widely used by radiobiology researchers and is therefore the most suitable for conducting this research.

It is difficult to measure absorbed dose to mice in vivo. It is even more difficult to measure such doses to mouse tumors in situ. Here, a phantom replica mouse has been chosen to quantify the dose received to living mice. The phantom mouse consisted of a white rubber polycarbonate material with a 7 cm body length, proportioned to be identical to that of the living mice shown in Fig. 1. The elemental composition is estimated as 85.6% amorphous carbon and 14.4% hydrogen, constituting a butyl solid of tissue-like density. Fig. 3 shows the mouse phantom bored out to accommodate various sized detectors. The detectors used in this research are presented to scale in Fig. 4.

As shown in Fig. 3, an ionization chamber was inserted into the back and pushed superiorly to the location of the left flank of the phantom mouse, where the sensitive volume appears flush with the outer skin

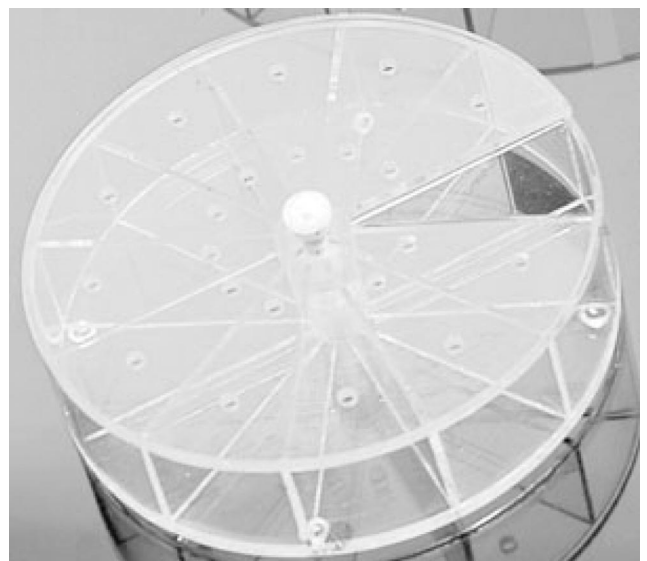


Fig. 2. Brain Tree Scientific Model pie cage No. MPC with MPC-TP filter.

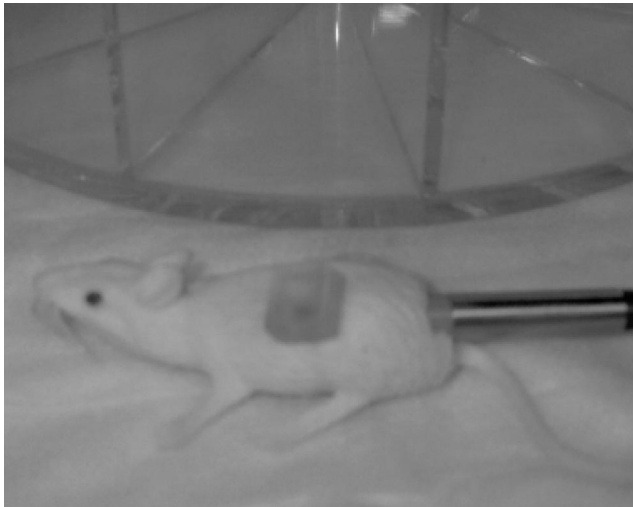


Fig. 3. Phantom mouse with bolus tumor simulating *in vivo* xenografted tumor and ionization chamber inserted.

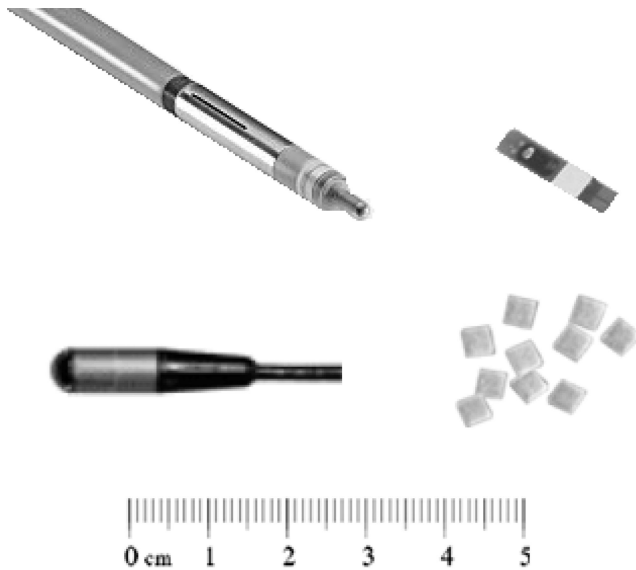


Fig. 4. Detectors used in the measurement of dose from left to right: at top—ionization chamber and MOSFET; at bottom—diode and TLDs.

layer. To imitate the resulting tumor growth on living mice, a bolus was cut and placed directly on the flank area, directly abutting the underlying detector's sensitive volume. The position of the detector thimble was easily seen through the transparent yellowish bolus material as illustrated (Fig. 3). A Radiation Products and Design, Inc. (RPD) (5218 Barthel Industrial, Albertville, MN 55301) tissue bolus prosthesis model 486-305 was used to simulate flanked nude mouse disease (Greco et al. 2010). With original factory dimensions $30 \text{ cm}^2 \times 0.5 \text{ cm}$, the rubber mold was cut down to $1 \text{ cm}^2 \times 0.5 \text{ cm}$ to

resemble the typical tumor size of a xenografted mouse used in these tumor biology studies.

The experiments were run consecutively for each detector used in this study. Each detector was specifically chosen based on size and importance for involvement in this study as observed in documented research (Stern 2009). A PTW (Lorracher Strasse 7, 79115 Freiburg, Germany) model TN31014 miniature thimble-type ionization chamber was used as shown in position in Fig. 3, having tip length 6.925 mm, width 3.4 mm, and sensitive volume 0.015 cm^3 . The ion chamber point of measurement was determined as the radius, located 1.7 mm from the outer thimble wall. The ion chamber was connected to CNMC Company, Inc. (865 Easthagen Dr., Nashville, TN 37215), model 206 with 200 nC module model 206-110 for measurements. The chamber was equilibrated to +300 V nominally at the center-pin.

The Sun Nuclear (425-A Pineda Court, Melbourne, FL 32940) Isorad-pTM diode model 1163000-1 was used, having diameter $7.1 \text{ mm} \times 29.5 \text{ mm}$ long with an 8.3-mm distance from tip to approximate point of measurement within the die. The diode point of measurement was determined as the radius, located 3.6 mm from the outer wall. The p-type diode was connected to a Nuclear Associates (100 Voice Rd., Carle Place, NY 11514) electrometer model 37-720 for measurements. The only requirement on the diode selected was to insure that it contained enough buildup so that the point of measurement was beyond the buildup region to maximum dose registered. Insuring that this was the case eliminated the majority of the electron contamination produced by the high-energy photon beams. In this research, a constant field size (largest) and a constant source-to-surface distance were set. A field size correction factor was needed for the diode. This value was determined to be $CF(FS) = 1.04$ and was included in the calculation of dose to cross-calibrate the diode's response. With the source-to-surface distance near 100 cm, the correction factor for it was determined to be $CF(SSD) = 1.00$.

A Sixel Technologies, Inc. (3800 Gateway Center Blvd., Morrisville, NC 27560) metal-oxide semiconductor field-effect transistor (MOSFET) model OneDoseTM was the third detector type used. Each transistor was 6 mm wide \times 33 mm long \times 0.9 mm thick. The MOSFET point of measurement was determined as the half-thickness, located 0.5 mm from the outer wall. Three were used in this study for constancy verification in the use of the device.

Finally, three Quantaflux, LLC (2537 N. Waynesville Road Lane, Oregonia, OH 45054), thermoluminescent dosimeter (TLD) chips were used; model TLD-100 including Harshaw Chemical Company (1000 Harvard

Ave., Cleveland, OH) LiF:Mg,Ti powder. Each ribbon had square dimensions $(3.2 \text{ mm})^2 \times 0.15 \text{ mm}$ thick. The TLD point of measurement was determined as the half-thickness, located 0.1 mm from the outer wall. Likewise, multiple TLD detectors provided constancy results in the use of this particular detector.

While the TLDs were provided and processed by the University of Wisconsin-Madison Accredited Dosimetry Calibration Laboratory (ADCL) (Madison, WI) with National Institute of Standards and Technology (NIST) (Gaithersburg, MD) traceability, the other three device types were cross-calibrated against an independent ADCL calibrated dosimeter system. Again, each detector was placed into the mouse phantom consecutively during the experiment, such that it resides directly underneath the tumor bolus. Once inserted, the phantom mouse and contained detector were placed into one section of the mouse cage and covered by the cage's rotating lid.

The remainder of the phantom setup included the necessary backscatter and buildup to duplicate treatment geometry. One CIRS, Inc. (2428 Alameda Ave., Norfolk, VA 23513), Plastic Water™ model PW-4050 phantom plate was chosen for backscatter. The plate was 5 cm thick and had a surface area of $40 \times 40 \text{ cm}^2$. It was positioned directly underneath the pie cage. For buildup anterior to the cage, the RPD tissue bolus prosthesis model 486-305 was again used having dimensions $(30 \text{ cm})^2 \times 0.5 \text{ cm}$ and in combination with model 486-310 having dimensions $(30 \text{ cm})^2 \times 1.0 \text{ cm}$ for a total of 1.5 cm depth equivalence. More dose uniformity resulted from the use of such bolus material, since off-axis horn effects from linear accelerator treatments are greatly reduced when x-rays traverse deeper in tissue.

CT acquisition

Scanning was obtained using a General Electric (GE) Lightspeed RT scanner (Fairfield, CT). The technique for scanning included 120 kVp x-rays, 150 mA current at a 1,950 ms scan time conducted in helical mode. A 50-cm-diameter circular field of view was used with a couch increment of 2.5 mm/slice. Once the scan was reconstructed, all 121 slices within the set were transferred to a treatment-planning computer.

Computerized tomography was conducted with the backscatter material, pie cage, and bolus material in position. The entire phantom set was placed on the CT couch and aligned by lasers such that the pie cage was centered in the beam and at a distance of 100 cm at the anterior surface. For CT acquisition only, no detector was inserted into the replica mouse. Instead, a substitute plastic rod was inserted. This step insured no dose was given to the MOSFET or TLD during scanning, since

both are sensitive enough to register unwanted dose during this imaging process. The plastic material was knowingly identifiable once the images were processed, allowing researchers to use the known dimensions of each device to contour and reconstruct each in the treatment planning system.

Computerized treatment simulation

A Varian Medical Systems, Inc. (3100 Hansen Way, Palo Alto, CA 94306), model Eclipse External Beam Planning Software version 8.1.20 was used to model the simulated dose distribution. Immediately following scan import, each slice was visually examined for artifacts. Special care was taken to identify and contour the pie cage on each slice, since much of the cage volume consists of air. The phantom mouse and bolus tumor were also 3-dimensionally contoured. Special care was taken to create new structures duplicating the dimensions of the four detectors used: ionization chamber, diode, MOSFET, and TLD.

The Varian Anisotropic Analytical Algorithm (AAA) version 8.6.15 was commissioned with heterogeneity correction for density enabled in the planning software, specifically for beam data corresponding to a Trilogy upgraded Varian model 21EX particle accelerator at photon energy 6 MV. An output calibration was performed prior to experimentation on the particle accelerator according to the AAPM Task Group No. 51 protocol (Almond et al. 1999). The calibration geometry included a source-to-surface distance of 98.5 cm in water and was defined by $10 \times 10 \text{ cm}^2$ radiation field size. The effective point of measurement for a reference ionization chamber at the depth of maximum dose was nominally 1.5 cm, such that the output determined at the axis of rotation for the machine (100 cm) was precisely 1.00 cGy for a 100-monitor unit delivery.

The radiation field was aimed anterior to the phantom set. The central axis of the beam was designed to pass directly through the center of the pie cage. The rotating canopy of the cage was set to the beam isocenter, located exactly 100 cm from the accelerator source. The resulting source-to-surface (SSD) distance at the bolus was 98.5 cm. The radiation field was defined by $40 \times 40 \text{ cm}^2$ jaw collimation, which easily envelopes the phantom, where beam properties of flatness and symmetry are ideal. The digitally reconstructed radiograph (DRR) illustrated in Fig. 5 indicates the phantom set is encompassed within the radiation field.

A dose calculation point was specifically set within the treatment planning system for the location of the detector. Each detector was positioned directly under the bolus material through the bore created in the mock-up

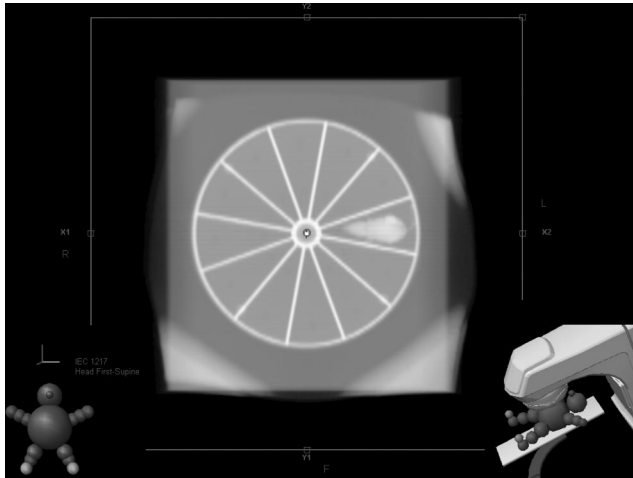


Fig. 5. Digitally reconstructed radiograph of the phantom set in the accelerator field.

mouse. The smallest possible dose calculation grid of 1.25 mm was assigned for best computational resolution. The computer algorithm was prescribed to receive 3 Gy at a rate of 6 Gy min^{-1} . The resulting isodose distribution is shown for the axial slice containing the phantom mouse in Fig. 6.

Radiation measurement

As previously discussed, the phantom system used was identical between simulation in the CT scanner and radiation measurement under the linear accelerator. A 1.5 cm-thick bolus buildup material was placed on top of the pie cage (having the phantom mouse and detector in place). Both were then laid on top of a 5-cm Plastic Water™ slab for sufficient backscatter. Beam geometry with the phantom placed on the couch of the accelerator was precisely the same as planned in simulation software. Again, lasers verified the position of the pie

cage-to-beam isocenter and with its centroid in line with the central axis of the beam. The accelerator jaws were fully opened and programmed to deliver radiation at a rate of 6 Gy min^{-1} using 6 MV x rays, for timer settings of 200 MU (monitor units), 300 MU, and 400 MU corresponding to calibrated doses of 2 Gy (200 cGy), 3 Gy (300 cGy), and 4 Gy (400 cGy).

RESULTS AND DISCUSSION

The density of the mouse phantom was determined to be very similar to tissue, with Hounsfield Units of $+135 \pm 30$. This leads to the conclusion that the mouse density corresponded to a range between adipose tissue ($-43 \pm 50 \text{ HU}$) with an electron density of $3.17 \times 10^{-23} \text{ e cm}^3 \text{ g cm}^{-3}$ and density 0.970 g cm^{-3} to that of liver ($+124 \pm 50 \text{ HU}$) with an electron density of $3.516 \times 10^{-23} \text{ e cm}^3$ and density 1.070 g cm^{-3} . Therefore, the phantom mouse chosen was estimated to be indistinguishable from a real mouse subject.

The analysis of the axial isodose plot in Fig. 6 shows an overall general symmetric shape to the dose distribution laterally. The isodose distribution was unique between wedged areas that contained the phantom mouse and those that did not. Therefore, the phantom mouse was seen to attenuate the beam. While the 100% isodose line passed directly through the axis of the phantom mouse on the right, the same isodose line existed on the left more posteriorly against the lower pie cage plate. Having identified the physical density of the phantom mouse to be similar to that of tissue, the attenuation effect on the beam that resulted was consistent.

Correctly computed, 100% of the dose was normalized to the posterior aspect of the tumor bolus. It is conclusive that a calculated absorbed dose of 3 Gy was received by the entirety of the tumor bolus for the given

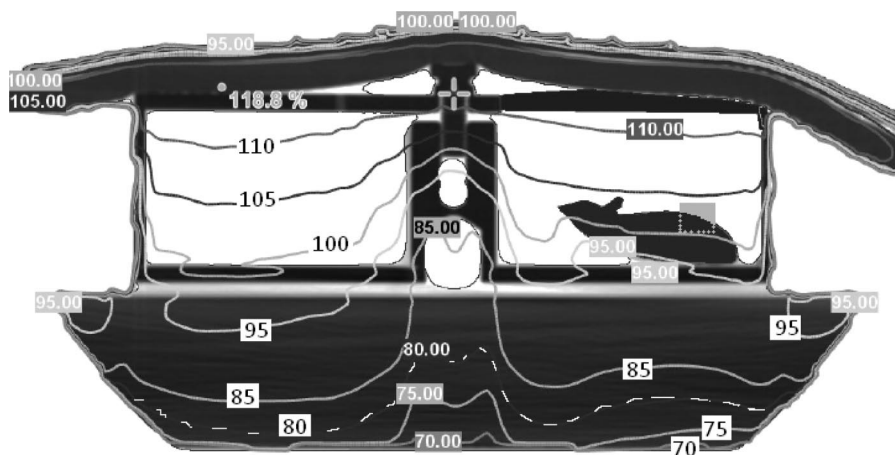


Fig. 6. Axial slice view with simulation software indicating the mathematically calculated dose levels in the pie cage.

time the beam was on. The planning simulation report concluded that 300 MU were required to yield a dose of 301 cGy. With a machine calibration of 1.00 cGy MU⁻¹ at the nominal distance of 1.5 cm and at beam isocenter, the dose to the mouse tumor was very nearly the same, even though substantially further away from the isocenter in the setup. The mouse phantom rested on the lower plate of the 7.5 cm-tall pie cage. The bolus on the mouse was only 3 cm from the posterior side of the lower pie cage plate. Thus, with beam isocenter aligned to the anterior surface of the pie cage, the tumor bolus was 4.5 cm further downstream from the isocenter. Having the same depth as that of calibration, yet further away from isocenter, the mouse tumor was expected to have lower dose calculated to it. According to a 1/r² fall-off for intensity, given [(100 cm + 1.5 cm)/(104.5 + 1.5 cm)]² = 0.917, one would expect approximately an 8.3% reduction in dose intensity. As this was not the case, the substantial air volume within the pie cage had caused equally as much increase in output. The cause could be found in the secondary electrons emitted in interactions induced in the top of the cage.

For the volume labeled “Tumor,” 100% of the 3 Gy dose was given to 100% of the tumor volume. As the

100% isodose line tracks through the axis of the phantom mouse, the dose to the whole mouse should be substantially less given the shallow curve representing its volume, labeled “Mouse” in Fig. 7. The dose volume histogram (DVH) also predicts similar doses should be received by the various detectors.

Reviewing the doses received by the detectors and depicted in Fig. 8, it becomes evident that the measured absorbed doses to the diode, TLDs, MOSFETs, and treatment planning system correlated well with the reference ionization chamber. The overall chamber response (n = 3) was determined to be reproducible to within a standard deviation of 0.3σ. The measurements of the ionization chamber were compared directly to each of the other systems.

The diode dose detection response (n = 3) was reproducible to within 0.5σ. It proved the most accurate with mean disagreement from the ion chamber of -0.4%. Less accurate measurements were obtained for the TLD chips and MOSFETs. The resulting precisions for these detectors were 2.6σ and 5.0σ, respectively. The mean measurement inaccuracy vs. the ionization chamber was found to be -2.4% for the TLDs (n = 3) and -2.9% for the MOSFET (n = 3). The worst among all

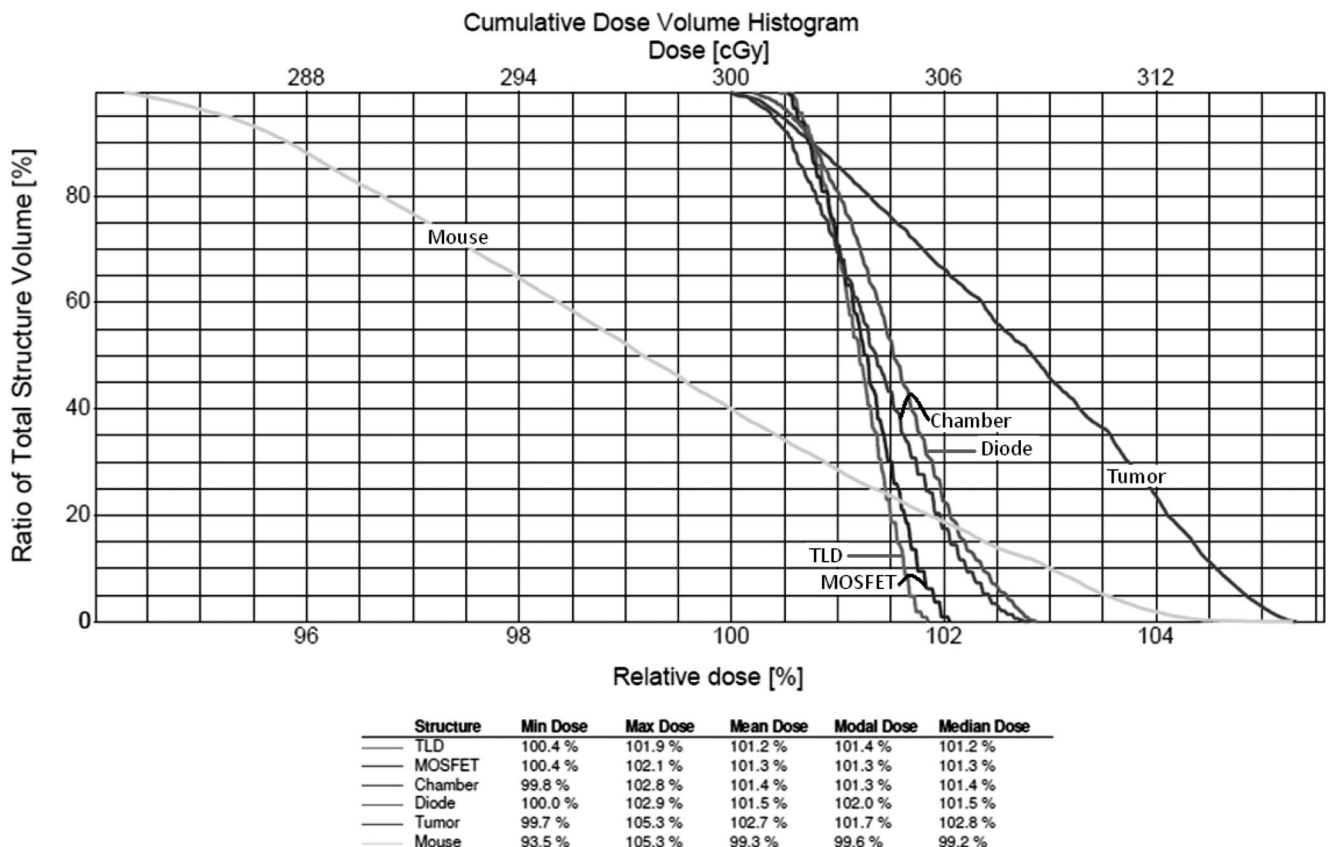


Fig. 7. Dose-volume histogram for all four detectors and including the mouse and tumor.

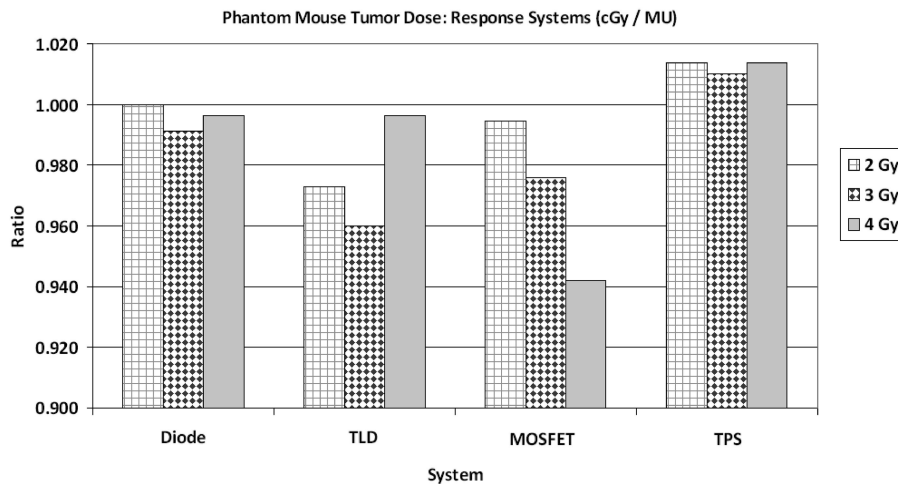


Fig. 8. Response of each detector type for phantom mouse tumor: Dose (cGy)/MU.

detectors was determined to be the MOSFET, although it was found to be reliable in estimating the dose to the tumor. All detector systems were found to underestimate the dose for all measurements in comparison to the accurate and precise calibrated ionization chamber response. The physical science of detection is different between these devices, due primarily to their design and construction, both of which enable the ionization chamber to be the most sensitive to charge collection rather than the diode, TLD, or MOSFET.

The treatment planning system was found to have reproducibility in its dose determination to within 1.3σ . Conversely, as seen from detector systems, the computer generally overestimated dose by comparison to the ion chamber. The treatment planning system ($n = 3$) accuracy fell within a mean disagreement from the ion chamber of $+1.3\%$.

CONCLUSION

This study introduces in vivo dose analysis of a radiobiologically studied mouse tumor, using a replica mouse phantom and tumor, both having a rubber density similar to that of adipose tissue or liver. A tumor volume created from bolus material overlaying a pre-bored cavity accommodating a dosimeter was introduced. With CT acquisition and computerized simulation, dose levels to the mouse structure and to the target phantom tumor were found to be accurate with respect to measurements. Further, commonly used detector systems including diodes, thermoluminescent dosimeters, MOSFETs, and a commercially available treatment planning system were intercompared to reference ionization chamber results. The average disagreement from an accelerator calibrated

output dose prescription in the range of 200–400 cGy were $-0.4\% \pm 0.5\sigma$ for the diode, $-2.4\% \pm 2.6\sigma$ for the TLD, $-2.9\% \pm 5.0\sigma$ for the MOSFET, and $+1.3\% \pm 1.4\sigma$ for the treatment planning system.

For a 300 MU delivery with the particle accelerator, a dose of 300–301 cGy was detected by all four detector systems within the calculated accuracy and standard deviation. Therefore, in the geometry employed, a general 1:1 correlation was seen between the number of monitor units programmed on a linear accelerator and the dose required at the location of a mouse tumor. These detector types have proven capable of precisely determining the output for mice in a pie cage treatment geometry. The treatment planning system is also a valuable tool, which may serve as a verification to visualize dose levels prior to being administered, where changes may be considered for asymmetries in the dose profile that may be unobserved otherwise.

For higher dose prescriptions of 8 Gy to mice tumors, it is possible to obtain this dose on a linear accelerator calibrated to 1.00 cGy MU^{-1} when run at 6 Gy min^{-1} for only 80 s, thus saving a significant amount of time for live nude mouse exposures conducted identically. The authors stress that although this setup resulted in the same dose for the number of monitor units programmed (i.e., 300 MU yielding 300 cGy), future investigations should be experimentally verified with radiation detectors in this manner prior to proceeding, as this may not be true for other geometries, equipment, and targets. This phantom mouse design is unique, simple, reproducible, and therefore recommended as a standard approach to dosimetry for radiobiological mouse studies using any of the detectors in this study, while understanding the observed accuracy of each.

The authors fully advocate this novel consideration of the use of the treatment planning system to model the dose to a mouse for planning purposes prior to irradiation similarly. The implantation of such dose evaluations prior to dose delivery is a necessary quality assurance step for humans, and as such should be used if available and evaluated for accurate radiobiology setup considerations.

Acknowledgements—We gratefully acknowledge the Marshall University Biochemistry and Microbiology & Surgery Departments for their support.

REFERENCES

- Agarwal JK, Ayappan P, Santhamma AV. Carcinogenic effect of radiation on the mouse embryo; physical aspects of radiation dosimetry. *Strahlentherapie* 150:618–623; 1975.
- Allam A, Perez LA, Huang P, Taghian A, Azinovic I, Freeman J, Duffy M, Eford J, Suit HD. The effect of the overall treatment time of fractionated irradiation on the tumor control probability of a human soft tissue sarcoma xenograft in nude mice. *Int J Radiat Oncol Biol Phys* 32:105–111; 1995.
- Almond PR, Biggs PJ, Coursey BM, Hanson WF, Huq MS, Nath R, Rogers DW. AAPM's TG-51 protocol for clinical reference dosimetry of high-energy photon and electron beams. *Med Phys* 26:1847–1870; 1999.
- Butson MJ, Rozenfeld A, Mathur JN, Carolan M, Wong TP, Metcalfe PW. A new radiotherapy dose detector: the MOSFET. *Med Phys* 23:655–658; 1996.
- Chia R, Achilli F, Festing MFW, Fisher EMC. The origins and uses of mouse outbred stocks. *Nature Genetics* 37:1181–1186; 2005.
- Gorodetsky R, Mou X, Fisher DR, Taylor JM, Withers HR. Radiation effect in mouse skin: dose fractionation and wound healing. *Int J Radiat Oncol Biol Phys* 18:1077–1081; 1990.
- Greco A, Benedetto AD, Howard CM, Kelly S, Nande R, Dementieva Y, Miranda M, Brunetti A, Salvatore M, Claudio L, Sarkar D, Dent P, Curiel DT, Fisher PB, Claudio PP. Eradication of therapy-resistant human prostate tumors using an ultrasound guided site-specific cancer terminator virus delivery approach. *Molecular Therapy* 18:295–306; 2010.
- Jaffe DR, Williamson JF, Tim G. Ionizing radiation enhances malignant progression of mouse skin tumors. *Carcinogenesis* 8:1753–1755; 1987.
- Kumar S, Kolozsvary A, Kohl R, Lu M, Brown S, Kim JH. Radiation-induced skin injury in the animal model of scleroderma: implications for post-radiotherapy fibrosis. *Radiat Oncol* 3:40; 2008.
- Kuroda M, Inamura K, Tahara S, Kurabayashi Y, Akagi T, Asaumi J, Togami I, Takemoto M, Honda O, Morioka Y, Kawasaki S, Hiraki Y. A new experimental system for irradiating tumors in mice using a linear accelerator under specific pathogen-free conditions. *Acta Med Okayama* 53:111–118; 1999.
- Lazewatsky J, Ding Y, Onthank D, Silva P, Solon E, Robinson S. Radiation dose to abdominal organs of the mouse due to ⁹⁰Y in the urinary bladder. *Cancer Biotherapy Radiopharmaceuticals* 18:413–419; 2003.
- Leiter EH. The NOD mouse: a model for analyzing the interplay between heredity and environment in development of autoimmune disease. *Institute for Lab Animal Research (ILAR)* 35(1); 1993.
- Lo Y, Taylor JMG, McBride WH, Withers HR. The effect of fractionated doses of radiation on mouse spinal cord. *Int J Radiat Oncol Biol Phys* 27:309–317; 1993.
- Lynch CJ. The so-called Swiss mouse. *Lab Animal Care* 19:214–220; 1969.
- Metcalfe P, Kron T, Elliott A, Wong T. Dosimetry of 6-MV x-ray beam penumbra. *Med Phys* 20:1439–1445; 1993.
- Morse III HC. *Origins of inbred mice*. Bethesda, MD: National Institute of Allergy and Infectious Diseases—National Institutes of Health; 1978.
- Quach KY, Morales J, Butson MJ, Rosenfeld AB, Metcalfe PE. Measurement of radiotherapy x-ray skin dose on a chest wall phantom. *Med Phys* 27:1676–1680; 2000.
- Stern RL. Dosimetry metrology for IMRT: Part I. *Med Phys* 36:2756; 2009.
- Stüben G, Budach W, Schick KH, Stuschke M, Stapper N, Müller S, Feldmann HJ. A time-saving system for irradiations of experimental tumors. *Strahlenther Onkol* 170:36–41; 1994.
- Suzuki N, Hirata M, Kondo S. Traveling stripes on the skin of a mutant mouse. *Proceedings of the National Academy of Sciences of the United States of America (PNAS)*. 100:9680–9685; 2003.
- Urano M, Nishimura Y, Kuroda M, Reynolds R. Are hypoxic cells critical for the outcome of fractionated radiotherapy in a slow-growing mouse tumor? *Radiotherapy Oncol* 48:221–228; 1998.
- Yorke E, Alecu R, Ding L, Fontenla D, Kalend A, Kaurin D, Masterson-McGary ME, Marinello G, Matzen T, Saini A, Shi J, Simon W, Zhu TC, Zhu XR, Rikner G, Nilsson G. AAPM Report No. 87—Report of Task Group 62 of the Radiation Therapy Committee: diode in vivo dosimetry for patients receiving external beam radiation therapy. Madison, WI: Medical Physics Publishing; 2005. ■ ■